relative to that in the poor responders (Fig. 6). Thus, the TBF map seems to be more useful for evaluating treatment response as compared with conventional static MR images alone, which are not reliable in differentiating viable tumors from treatment-induced changes.

Tumor blood flow increased as a result of angiogenesis, but the increased TBF did not directly reflect the angiogenesis. Nonetheless, the TBF map clearly showed the heterogeneity of perfusion in the tumor, that is, higher on the periphery and lower in the center of the tumor. Similar images were previously reported in experimental animal studies[13] and in human breast cancers,[27] in which peripheral enhancement in invasive carcinoma correlated with high peripheral microvessel densities reflecting tumor angiogenesis.[27] We did not measure the microvascular density in this study; however, there have been reports concerning the comparison between the physiological findings such as microvascular density compared with the DCE-MRI measurements. Verstraete et al[22] reported that the degree of vascularization estimated by factor VIII staining (which better reflected the tumor angiogenesis) obtained from pathological specimens significantly correlated with the first-pass slope values obtained from the DCE-MRI measurements in musculoskeletal lesions. In breast lesions, Buadu et al[27] also reported that the density and distribution of microvessels were correlated with the time-intensity curve types and the slope values obtained from the DCE-MRI measurements. We believe that the increased TBF demonstrated in the TBF maps in this study would correspond to the increased density of microvessels and, thus, better reflect tumor angiogenesis.

In conclusion, we could successfully generate a functional map of TBF with high temporal and spatial resolutions. Tumor blood flow maps clearly demonstrated wide variances and heterogeneity of blood flow in tumors, and substantial decreases in TBF were demonstrated after chemotherapy. Although it is definitely warranted to validate the quantitative values and to further evaluate TBF maps in a larger number of patients with various tumors, assessment of TBF by DCE-MRI and deconvolution analysis would be promising for noninvasively evaluating TBF in vivo and for monitoring treatment response.

REFERENCES

1. Folkman J. Tumor angiogenesis: therapeutic implications. *N Engl J Med.* 1971;285:1182–1186.
2. Weidner N, Semple JP, Welch WR, et al. Tumor angiogenesis and metastasis-correlation in invasive breast carcinoma. *N Engl J Med.* 1991;324:1–8.
3. Wiggins DL, Granai CO, Steinhoff MM, et al. Tumor angiogenesis as a prognostic factor in cervical carcinoma. *Gynecol Oncol.* 1995;56: 353–356.
4. Gasparini G, Harris AL. Clinical importance of the determination of tumor angiogenesis in breast carcinoma: much more than a new prognostic tool. *J Clin Oncol.* 1995;13:765–782.
5. Folkman J. New perspectives in clinical oncology from angiogenesis research. *Eur J Cancer.* 1996;32A:2534–2539.
6. Pluda JM. Tumor-associated angiogenesis: mechanisms, clinical implications, and therapeutic strategies. *Semin Oncol.* 1997;24: 203–218.
7. Delorme S, Knopp MV. Non-invasive vascular imaging: assessing tumour vascularity. *Eur Radiol.* 1998;8:517–527.
8. Anderson H, Price P. Clinical measurement of blood flow in tumours using positron emission tomography: a review. *Nucl Med Commun.* 2002;23:131–138.
9. Ruotsalainen U, Raitakari M, Nuutila P, et al. Quantitative blood flow measurement of skeletal muscle using oxygen-15-water and PET. *J Nucl Med.* 1997;38:314–319.
10. Tofts PS, Kermode AG. Measurement of the blood-brain barrier permeability and leakage space using dynamic MR imaging. 1. Fundamental concepts. *Magn Reson Med.* 1991;17:357–367.
11. Brix G, Semmler W, Port R, et al. Pharmacokinetic parameters in CNS Gd-DTPA enhanced MR imaging. *J Comput Assist Tomogr.* 1991;15: 621–628.
12. Ostergaard L, Weisskoff RM, Chesler DA, et al. High resolution measurement of cerebral blood flow using intravascular tracer bolus passages. Part I: mathematical approach and statistical analysis. *Magn Reson Med.* 1996;36:715–725.
13. Pahernik S, Griebel J, Botzlar A, et al. Quantitative imaging of tumour blood flow by contrast-enhanced magnetic resonance imaging. *Br J Cancer.* 2001;85:1655–1663.
14. Meier P, Zierler KL. On the theory of the indicator-dilution method for measurement of blood flow and volume. *J Appl Physiol.* 1954;6: 731–744.
15. Rosen G, Caparros B, Huvos AG, et al. Preoperative chemotherapy for osteogenic sarcoma: selection of postoperative adjuvant chemotherapy based on the response of the primary tumor to preoperative chemotherapy. *Cancer.* 1982;49:1221–1230.
16. Murase K, Kikuchi K, Miki H, et al. Determination of arterial input function using fuzzy clustering for quantification of cerebral blood flow with dynamic susceptibility contrast-enhanced MR imaging. *J Magn Reson Imaging.* 2001;13:797–806.
17. Fritz-Hansen T, Rostrup E, Larsson HB, et al. Measurement of the arterial concentration of Gd-DTPA using MRI: a step toward quantitative perfusion imaging. *Magn Reson Med.* 1996;36:225–231.
18. Kikuchi K, Murase K, Miki H, et al. Quantitative evaluation of mean transit times obtained with dynamic susceptibility contrast-enhanced MR imaging and with (133)Xe SPECT in occlusive cerebrovascular disease. *AJR Am J Roentgenol.* 2002;179:229–235.
19. Ohno Y, Hatabu H, Murase K, et al. Quantitative assessment of regional pulmonary perfusion in the entire lung using three-dimensional ultrafast dynamic contrast-enhanced magnetic resonance imaging: preliminary experience in 40 subjects. *J Magn Reson Imaging.* 2004;20: 353–365.
20. Purdie TG, Henderson E, Lee TY. Functional CT imaging of angiogenesis in rabbit VX2 soft-tissue tumour. *Phys Med Biol.* 2001;46:3161–3175.
21. Hudlicka O. Regulation of muscle blood flow. *Clin Physiol.* 1985;5: 201–229.
22. Verstraete KL, De Deene Y, Roels H, et al. Benign and malignant musculoskeletal lesions: dynamic contrast-enhanced MR imaging-parametric "first-pass" images depict tissue vascularization and perfusion. *Radiology.* 1994;192:835–843.
23. van der Woude HJ, Bloem JL, Verstraete KL, et al. Osteosarcoma and Ewing's sarcoma after neoadjuvant chemotherapy: value of dynamic MR imaging in detecting viable tumor before surgery. *AJR Am J Roentgenol.* 1995;165:593–598.
24. Verstraete KL, Van der Woude HJ, Hogendoorn PC, et al. Dynamic contrast-enhanced MR imaging of musculoskeletal tumors: basic principles and clinical applications. *J Magn Reson Imaging.* 1996; 6:311–321.
25. Dyke JP, Panicek DM, Healey JH, et al. Osteogenic and Ewing sarcomas: estimation of necrotic fraction during induction chemotherapy with dynamic contrast-enhanced MR imaging. *Radiology.* 2003;228: 271–278.
26. Erlemann R, Sciuk J, Bosse A, et al. Response of osteosarcoma and Ewing sarcoma to preoperative chemotherapy: assessment with dynamic and static MR imaging and skeletal scintigraphy. *Radiology.* 1990;175: 791–796.
27. Buadu LD, Murakami J, Murayama S, et al. Breast lesions: correlation of contrast medium enhancement patterns on MR images with histopathologic findings and tumor angiogenesis. *Radiology.* 1996; 200:639–649.

Radiat Med (2006) 24:159–164
DOI 10.1007/s11604-005-0001-2

ORIGINAL ARTICLE

Assessment of left ventricular wall motion using 16-channel multislice computed tomography: comparison with left ventriculography

Toyoaki Haraikawa · Hiroshi Higashino
Yoshifumi Sugawara · Hitoshi Miki · Akira Kurata
Jitsuo Higaki · Teruhito Mochizuki

Received: December 20, 2004 / Accepted: October 28, 2005

Abstract
Purpose. Using the raw data from coronary computed tomography (CT) angiography, multislice CT (MSCT) can be used to evaluate cardiac function. However, the accuracy of left ventricular (LV) wall motion assessment by MSCT has not been thoroughly investigated. We investigated whether 16-channel MSCT could accurately assess LV wall motion by comparing its results with those of conventional biplane left ventriculography (LVG).
Materials and methods. The study included 20 patients with various kinds of heart disease. All patients underwent both contrast-enhanced MSCT and biplane LVG. Using a retrospective electrocardiography-gating technique, 10 phases over one cardiac cycle were extracted. The left ventricle was divided into seven segments according to the American Heart Association classification. Wall motion was scored as follows: 1, normal; 2, mild to moderate hypokinesis; 3, severe hypokinesis; 4, akinesis; 5, dyskinesis; and 6, aneurysm. The scores obtained by MSCT were compared with those obtained by LVG. The wall motion scores were analyzed using the chi-squared independence test (6 × 6 contingency table).
Results. Wall motion could be assessed in all segments of the 20 patients using interactive multiplanar animation. Among a total of 140 segments in 20 patients, scores in 118 were concordant between MSCT and LVG (118/140, 84.3%).
Conclusion. The 16-MSCT can accurately assess LV wall motion.

Key words Multislice CT · Cardiac imaging · Left ventricular function · Left ventricular wall motion · Left ventriculography

T. Haraikawa · H. Higashino (✉) · Y. Sugawara · H. Miki · T. Mochizuki
Department of Radiology, Ehime University School of Medicine, Shitsukawa, Toon, Ehime 791-0295, Japan
Tel. +81-89-960-5372; Fax +81-89-960-5375
e-mail: doctor@higashino.com

A. Kurata · J. Higaki
Second Department of Internal Medicine, Ehime University School of Medicine, Ehime, Japan

Introduction

Using single-detector helical computed tomography (CT), we developed a new application in which animated movies of two-dimensional (2D) cardiac axes and three-dimensional (3D) images were extracted retrospectively using the raw data derived by coronary CT angiography (CTA).[1–5] The animated movies allowed assessment of left ventricular (LV) wall motion and systolic wall thickening of the whole heart. With the development of multislice CT (MSCT), clearer cardiac imaging of the coronary artery has become available with thinner slices.[6,7] Coronary CTA has also become practical with more accurate assessability.[8–13] Because our application uses the same data as that for coronary CTA, no additional radiation exposure is needed.[14–16] If LV wall motion can be assessed accurately by MSCT, supplementing the information provided by coronary CTA, it would be beneficial in the clinical setting.[17,18] However, the accuracy of LV wall motion assessment by MSCT has not been well investigated. Therefore, we investigated whether 16-channel MSCT could assess LV wall motion by comparing its results with those gained by conventional biplane left ventriculography (LVG).

Table 1. Patient characteristics

Patient no.	Age (years)	Sex	Disease	Interval between MSCT and LVG (days)	Heart rate[a]
1	69	M	OMI (RCA, LCX)	31	Low
2	71	M	OMI (LAD)	3	Mid
3	64	M	AP	114	High
4	58	M	AP	15	Low
5	79	F	AP	76	High
6	69	F	AP	1	Low
7	69	F	AP	21	Mid
8	70	M	HCM	63	Mid
9	69	M	AP	26	Low
10	61	M	AMI (RCA)	5	Low
11	62	M	OMI (LAD)	2	Low
12	65	M	AP	1	Low
13	44	M	HCM	1	Low
14	68	M	ICM	1	Mid
15	72	F	SSS	1	Mid
16	76	F	AMI (LAD)	8	Low
17	68	M	MR	6	Low
18	75	F	AP	45	High
19	66	F	AP	7	Low
20	75	F	AP	3	Low

MSCT, multislice computed tomography; LVG, left ventriculography; OMI, old myocardial infarction; AP, angina pectoris; HCM, hypertrophic cardiomyopathy; AMI, acute myocardial infarction, ICM, ischemic cardiomyopathy; SSS, sick sinus syndrome; MR, mitral regurgitation; LAD, left anterior descending artery; LCX, left circumflex artery; RCA, right coronary artery

[a] Low, ≤60 beats/min; Mid, 61–75 beats/min; High, >75 beats/min

Materials and methods

Patient population

The study included 20 patients with various kinds of heart disease (10 patients with angina pectoris, 3 with old myocardial infarction, 2 with acute myocardial infarction, 2 with hypertrophic cardiomyopathy, 1 with ischemic cardiomyopathy, 1 with mitral regurgitation, and 1 with sick sinus syndrome). All patients underwent both MSCT for coronary CTA and conventional LVG. The mean age of the patients was 67.5 years. The mean intervals for MSCT and LVG were 21.5 days. Other patient characteristics are summarized in Table 1.

Data acquisition and processing of MSCT

The 16-channel MSCT instrument used was a LightSpeed Ultra 16 (GE Healthcare, Milwaukee, WI, USA) (gantry rotation speed 0.5 s/rotation). The scan protocol was the same as for coronary CTA. A beta-blocker (atenolol 50 mg, po) was administered 3 h before data acquisition to reduce the patient's heart rate for improved relative temporal resolution, which enables image production with fewer motion artifacts.[6] Data acquisition was performed while the patient held their breath at inspiration preceded by inhalation of oxygen (3 l/min). Patients lay on the scan table in the supine position; a noncontrast localization scan was performed first. Scan timing was determined with a test injection, using 15 ml (3 ml/s when body weight was <60 kg) or 20 ml (4 ml/s when body weight was ≥60 kg) of the contrast medium (300 mg iodine/ml) before the real scan. About 80 ml (body weight <60 kg) or 125 ml (body weight ≥60 kg) of contrast medium was injected at a rate of 3–4 ml/s. Each scan took about 20 s to cover the entire heart with a slice thickness of 0.625 mm.

To generate a moving image of the heart, 10 cardiac phase data sets were extracted using helical data acquisition (pitch 0.275–0.325), and a retrospective electrocardiography (ECG)-gating technique.

The MSCT scan mode was changed according to the heart rate (HR). When the HR was ≤60 beats/min (low-HR group), the "snapshot segment mode" (helical pitch 0.325) was used. When the HR was 61–75 beats/min (mid-HR group), the "burst mode" (helical pitch 0.3) was used. When the HR was >75 beats/min (high-HR group), the "burst plus mode" (helical pitch 0.275) was used.

Workstations for MSCT

Workstations used were Advantage Workstation 4.2 (GE Medical Systems, Milwaukee, WI, USA) and Zio M900 (Zio Software, Tokyo, Japan).

Data acquisition and processing of LVG

The biplane angiographic system used was a KXO-80C (Toshiba Medical System, Tokyo, Japan). Contrast medium (300 mg iodine/30 ml, 10 ml/s) was injected into the left ventricle, after which LVG was acquired at a frame rate of 30 images/s with a 512 × 512 matrix. The biplane LVG images in right anterior oblique 30 degrees (RAO30) and left anterior oblique 60 degrees (LAO60) were obtained.

Evaluation of image quality

Before analyzing LV wall motion, the image quality of MSCT was evaluated visually by the consensus of two readers as: 1, excellent; 2, good; 3, acceptable; or 4, poor (nonassessable).

Assessment of LV wall motion

To assess LV wall motion, the left ventrich was divided into seven segments according to the American Heart Association (AHA) classification in RAO30 and LAO60 (Fig. 1).[19]

With the two observers in agreement (T.H., A.K.), LV wall motion was visually evaluated and scored as: 1, normal; 2, mild to moderate hypokinesis; 3, severe hypokinesis; 4, akinesis; 5, dyskinesis; 6, aneurysm. The biplane animated images of LVG in RAO30 and LAO60 were applied to assess LV wall motion.

The multiplanar reconstructed (MPR) animated images of MSCT in RAO30 and LAO60 were generated in the workstation. Because the thickness of the MPR image was 0.625 mm, the multiple parallel MPR images along RAO30 and LAO60 was applied for assessment.

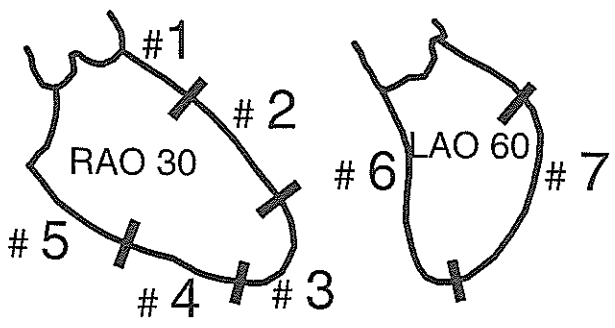

Fig. 1. Left ventricular (LV) wall segmentation according to the American Heart Association (AHA) classification (1975 AHA committee report): *1*, anterobasal wall; *2*, anterolateral wall; *3*, apical wall; *4*, diaphragmatic or inferior wall; *5*, posterobasal wall; *6*, septal wall; *7*, posterolateral wall *RAO*, right anterior oblique; *LAO*, left anterior oblique

The motion of the endocardial border was evaluated in the same manner as the LVG.

MSCT scoring of all patients was performed first. Scoring of LVG was performed next and independently.

Data analysis

The MSCT and LVG scores were compared, and the agreement between the two modalities was investigated with the chi-squared independence test (6 × 6 contingency table). All statistical analyses were performed using SPSS software (version 11.1; SPSS, Chicago, IL, USA). $P < 0.05$ was considered statistically significant.

Results

Observation of LV wall motion was possible in all 20 patients. For visual assessment, the image quality was excellent for six patients (30%), good for nine patients (45%), acceptable for five patients (25%), and poor for 0 patients.

The LV wall motion scores for each segment are given in Table 2. The overall agreement in scores between MSCT and LVG was 84.3% (118/140) (Table 3, Fig. 2). The MSCT findings were normal in 89 of 98 LVG normal segments (89/98, 90%). The LV wall motion scores did not match in 22 segments, but the difference was only one point (Fig. 3) in all but one segment, where the difference was two points. Matching of the LV wall motion scores was slightly worse in AHA segments 4, 6, and 7, but there were no significant differences.

Discussion

The good agreement of the LV wall motion scores between MSCT and LVG indicates that MSCT can accurately assess wall motion. Although we compared two modalities—2D projection images (LVG) and tomographic or 3D images (MSCT)—we did not encounter any difficulty as we used similar directions for evaluating of the LV wall motion generated by MSCT.

In 22 segments, however, LV wall motion scores by MSCT did not agree with those obtained by LVG. The discrepancy between MSCT and LVG results may have been caused in part by the lower temporal resolution of MSCT.

We applied a beta-blocker to improve temporal resolution, and use of the beta-blocker might have affected cardiac function. The contrast opacity of LVG may be lower in apical and inferior (RAO60) and septal and lateral (LAO60) segments, but the contrast of the LV

Table 2. Wall motion score

Patient no.	MSCT image quality	LVG score, by wall segments 1–7[a]							MSCT score, by wall segments 1–7[a]						
		1	2	3	4	5	6	7	1	2	3	4	5	6	7
1	Acceptable	1	1	1	2	3	1	2	1	2	2	1	3	2	1
2	Excellent	2	2	2	1	1	3	1	2	2	2	1	1	2	1
3	Excellent	1	1	1	1	1	1	1	1	1	1	1	1	1	1
4	Good	1	1	1	1	1	1	1	1	1	1	1	1	1	1
5	Excellent	1	2	2	2	1	1	1	1	2	2	2	1	1	1
6	Good	1	2	2	1	1	1	1	1	2	2	2	1	2	1
7	Excellent	1	2	2	1	1	2	1	1	2	2	1	1	2	1
8	Excellent	1	1	1	1	1	1	1	1	1	1	1	1	1	1
9	Good	1	1	1	1	1	1	1	1	1	1	1	1	1	1
10	Good	1	1	6	3	3	1	3	1	1	6	2	2	1	1
11	Good	1	2	2	1	1	2	1	1	2	2	1	1	2	1
12	Acceptable	1	3	3	2	5	1	2	1	3	3	2	5	1	3
13	Good	1	1	1	1	1	1	1	1	1	1	1	1	1	1
14	Excellent	3	3	3	2	4	2	5	3	3	3	3	4	2	4
15	Good	1	1	1	1	1	1	1	1	1	1	1	1	1	1
16	Acceptable	2	3	4	2	2	3	1	2	3	4	3	2	3	2
17	Acceptable	1	1	1	1	1	1	1	1	1	1	1	1	1	1
18	Good	1	1	1	1	1	1	1	2	2	1	2	1	1	1
19	Good	1	1	2	1	1	1	1	1	1	2	2	1	2	1
20	Acceptable	1	1	2	1	1	1	1	1	2	2	1	1	1	1

[a] According to the American Heart Association classification
Data are wall motion scores for each of the segments (1–7)

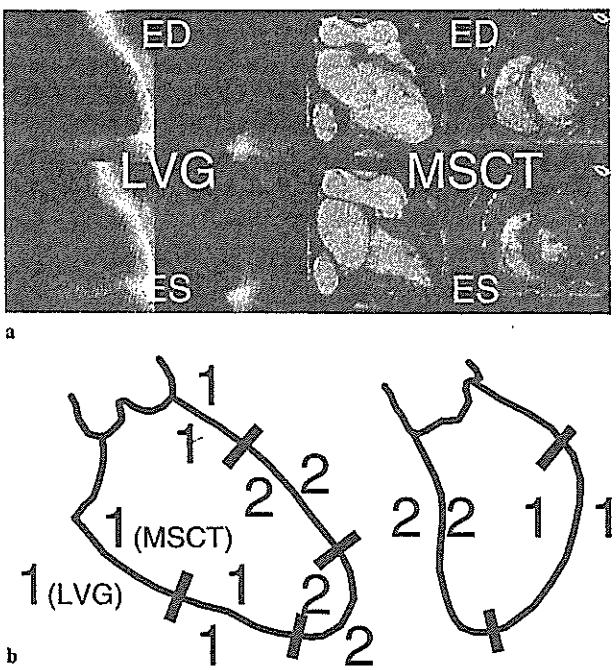

Fig. 2. A 69-year-old woman with angina pectoris (patient 7). Left venticulography (*LVG*) and multi-slice computed tomography (MSCT) (image quality excellent) showed mild hypokinesis in left anterior descending coronary artery (LAD) territory (**a**). LV wall motion scores (**b**) between MSCT (*inside panels*) and LVG (*outside panels*) agreed in all segments. *ED*, end-diastole; *ES*, end-systole

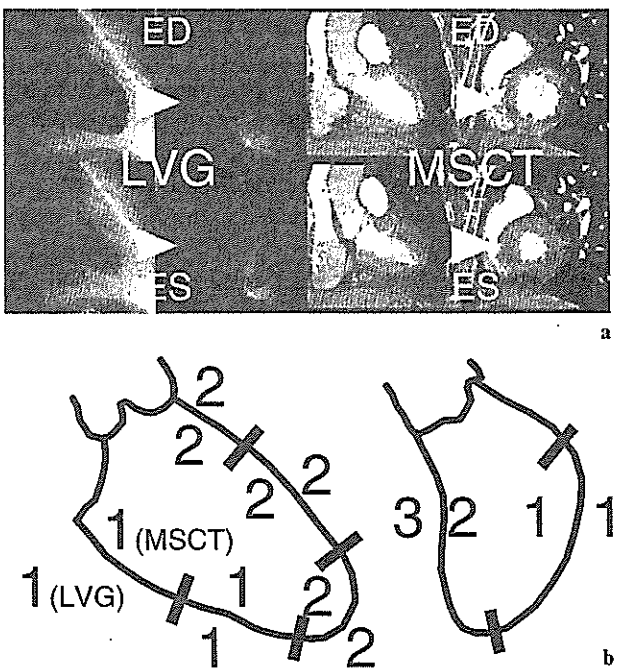

Fig. 3. A 71-year-old man with an old myocardial infarction (patient 13). The LVG and MSCT (image quality acceptable) showed mild or moderate hypokinesis in LAD territory (**a**). There was a mismatch of the LV wall motion score (**b**) between MSCT (*inside panels*) and LVG (*outside panels*) in the septal wall (*6* in Fig. 1) (*arrow*)

Table 3. Comparison of MSCT and LVG wall motion scores

LVG wall motion score	No. of segments with MSCT wall motion scores 1–6						
	1	2	3	4	5	6	Total
1	86	12	0	0	0	0	98
2	2	20	3	0	0	0	25
3	1	3	8	0	0	0	12
4	0	0	0	2	0	0	2
5	0	0	0	1	1	0	2
6	0	0	0	0	0	1	1
Total	89	35	11	3	1	1	140

cavity to the myocardium with MSCT was usually high, which might be another cause of the discrepancy.

The LVG images were maximum projection data for the LV cavity, whereas the MSCT data are for both the LV cavity and the myocardium. When assessing LV wall motion by MSCT, systolic wall thickening was observed, which might be another cause of the discrepancy.

The patients were classified into three groups of temporal resolution: 12 patients in the low-HR group, 5 in the mid-HR group, and 3 in the high-HR group. There were no significant correlations between the wall motion discrepancy and the temporal resolution.

The maximum interval of MSCT and LVG was 114 days, and in three patients the intervals were more than 2 months. These three patients had chronic disease but were stable, and the MSCT and LVG scores agreed completely.

The matching of motion scores was slightly worse in segments 4, 6, and 7, which might be affected by LVG characteristics. In RAO30 the opacity of the apical and inferior LV border was lower, and in LAO60 the long septal and lateral lines were projected to short lines of maximun intensity projection (MIP) images.

In segment 7 of case 14, the LV motion score of MSCT indicated akinesis, whereas that of LVG indicated dyskinesis. Assessment of LV wall motion by LVG was performed by evaluating the border of MIP images of the whole heart; in contrast, assessment with MSCT was performed by evaluating multiple parallel 0.625-mm-thick MPR images. This discrepancy in the motion scores may be affected by the differences of the objects.

Each of the noninvasive cardiac imaging modalities, such as echocardiography, ECG-gated single photon emission CT, and cine magnetic resonance imaging, has its own advantages.[20] The advantages of MSCT are its ready availability, short acquisition time (20 s with 16-channel MSCT), and high spatial resolution. MSCT can assess LV wall motion retrospectively in any direction with 2D animation of cardiac axes or 3D images. A smooth animated movie was obtained with 10 frames of one cardiac cycle.

Although MSCT requires radiation exposure and contrast medium, the same raw data as used for coronary CTA can be used for MSCT.[1–5,14–18,21] Therefore, no additional irradiation is necessary. In other words, the greatest advantage of MSCT is that LV wall motion assessment is available with coronary CTA without additional radiation exposure. Because the image quality of coronary CTA has been improving rapidly with the development of the MSCT system in terms of temporal and spatial resolution, coronary CTA has become a new tool for noninvasive coronary artery imaging.[6,7] Thus, the more clinically useful coronary CTA becomes, the more practical MSCT becomes for noninvasive evaluation of LV wall motion and other functional assessments.[8–13]

We applied 10 frames for visual assessment in this study, but it is unclear whether this number is suitable for quantitative assessment of LV wall motion (as the regional ejection fraction) and of systolic thickening (as percent wall thickening). Proper framing of a quantitative assessment of cardiac function should be addressed in a future study.

Limitations

A total of 192 slices were reconstructed to cover the entire heart (12 cm) in the head-to-foot direction at intervals of 0.625 mm. To reconstruct 10 phases, 1920 slices were necessary. The handling of this many slices requires rapid reconstruction speed, rapid transfer of the slice data to the workstation, and rapid loading with a large amount of memory. A sophisticated workstation and software to handle all the data and to generate moving images are also necessary. We speculate that the clinical requirements will accelerate the development of a powerful workstation and sophisticated software.

Conclusion

Interactive animated movies by MSCT provide a new noninvasive means to assess LV wall motion using the same data as for coronary CTA.

References

1. Mochizuki T, Murase K, Higashino H, Koyama Y, Doi M, Miyagawa M, et al. Two- and three-dimensional CT ventriculography: a new application of helical CT. AJR Am J Roentgenol 2000;174:203–8.

2. Mochizuki T, Higashino H, Koyama Y, Hosoi S, Tsuda T, Sugawasa Y, et al. Clinical usefulness of the cardiac multidetector-row CT. Comput Med Imaging Graph 2003;27:35–42.
3. Mochizuki T, Hosoi S, Higashino H, Koyama Y, Mima T, Murase K. Assessment of coronary artery and cardiac function using multidetector CT. Semin Ultrasound CT MRI 2004;25:99–112.
4. Koyama Y, Mochizuki T, Higaki J. Computed tomography assessment of myocardial perfusion, viability, and function. J Magn Reson Imaging 2004;19:800–15.
5. Hosoi S, Mochizuki T, Miyagawa M, Shen Y, Murase K, Ikezoe J. Assessment of left ventricular volumes using multidetector row computed tomography (MSCT): phantom and human studies. Radiat Med 2003;21:62–7.
6. Flohr T, Bruder H, Stierstorfer K, Simon J, Schaller S, Ohnesorge B. New technical developments in multislice CT. Part 2. Sub-millimeter 16-slice scanning and increased gantry rotation speed for cardiac imaging. Rofo 2002;174:1022–7.
7. Kopp AF, Schroeder S, Kuettner A, Heuschmid M, Georg C, Ohnesorge B, et al. Coronary arteries: retrospectively ECG-gated multi-detector row CT angiography with selective optimization of the image reconstruction window. Radiology 2001;221:683–8.
8. Achenbach S, Ulzheimer S, Baum U, Kachelriess M, Ropers D, Giesler T, et al. Noninvasive coronary angiography by retrospectively ECG-gated multislice spiral CT. Circulation 2000;102:2823–8.
9. Achenbach S, Giesler T, Ropers D, Ulzheimen S, Derlien H, Schulte C, et al. Detection of coronary artery stenoses by contrast-enhanced, retrospectively electrocardiographically-gated, multislice spiral computed tomography. Circulation 2001;103:2535–8.
10. Kopp AF, Schroeder S, Kuettner A, Baumbach A, Georg C, Kuzo R, et al. Non-invasive coronary angiography with high resolution multidetector-row computed tomography: results in 102 patients. Eur Heart J 2002;23:1714–25.
11. Sato Y, Matsumoto N, Kato M, Inoue F, Horie T, Kusama J, et al. Noninvasive assessment of coronary artery disease by multislice spiral computed tomography using a new retrospectively ECG-gated image reconstruction technique: comparison with angiographic results. Circ J 2003;67:401–5.
12. Maruyama T, Yoshizumi T, Tamura R, Takashima S, Toyoshima H, Konishi I, et al. Comparison of visibility and diagnostic capability of noninvasive coronary angiography by eight-slice multidetector-row computed, tomography versus conventional coronary angiography. Am J Cardiol 2004;93: 537–42.
13. Schoepf UJ, Becker CR, Ohnesorge BM, Yucel EK. CT of coronary artery disease. Radiology 2004;232:18–37.
14. Cohnen M, Poll L, Puttmann C, Ewen K, Modder U. Radiation exposure in multi-slice CT of the heart. Rofo 2001;173: 295–9.
15. Poll LW, Cohnen M, Brachten S, Ewen K, Modder U. Dose reduction in multi-slice CT of the heart by use of ECG-controlled tube current modulation ("ECG pulsing"): phantom measurements. Rofo, 2002;174:1500–5.
16. Kyongtae TB, Cheng H, Bruce RW. Radiation dose in multidetector row computed tomography cardiac imaging. J Magn Reson Imaging, 2004;19:859–63.
17. Higashino H, Mochizuki T, Haraikawa T, Kurata A, Teruhito K, Nakata S, et al. Image fusion of coronary tree and regional cardiac function image using multislice computed tomography. Circ J 2006;70:105–9.
18. Lembcke A, Dushe S, Enzweiler CN, Kloeters C, Wiese TH, Hermann KG, et al. Passive external cardiac constraint improves segmental left ventricular wall motion and reduces akinetic area in patients with non-ischemic dilated cardiomyopathy. Eur J Cardio thorac Surg 2004;25:84–90.
19. Austen WG, Edwards JE, Frye RL, Gensini GG, Gott VL, Griffith LS, et al. A reporting system on patients evaluated for coronary artery disease: report of the Ad Hoc Committee for Grading of Coronary Artery Disease, Council on Cardiovascular Surgery, American Heart Association. Circulation 1975;51:5–40.
20. Bax JJ, Lamb H, Dibbets P, Pelikan H, Boersma E, Viergever EP, et al. Comparison of gated single-photon emission computed tomography with magnetic resonance imaging for evaluation of left ventricular function in ischemic cardiomyopathy. Am J Cardiol, 2000;86:1299–305.
21. Kurata A, Mochizuki T, Koyama Y, Haraikawa T, Suzuki J, Shigematsu Y, et al. Myocardial perfusion imaging using adenosine triphosphate stress multi-slice spiral computed tomography: alternative to stress myocardial perfusion scintigraphy. Circ J 2005;69:550–7.

Radiat Med (2006) 24:520–524
DOI 10.1007/s11604-006-0060-z

CASE REPORT

Subcutaneous fibrolipoma in the back

Makoto Kajihara · Yoshifumi Sugawara
Kenshi Sakayama · Yasuhito Abe · Hitoshi Miki
Teruhito Mochizuki

Received: January 5, 2006 / Accepted: April 11, 2006

Abstract A 65-year-old man presented with a subcutaneous giant mass in his upper back. The tumor had a massive fatty and nonadipose component that enhanced heterogeneously on contrast-enhanced computed tomography and magnetic resonance imaging. Therefore, the lesion was initially thought to be a liposarcoma or spindle cell lipoma. After surgery, the tumor was histologically diagnosed as a fibrolipoma. Subcutaenous fibrolipoma is a rare neoplasm that is defined as a subtype of lipoma.

Key words Fibrolipoma · Lipoma · Liposarcoma · MRI · CT

Introduction

Subcutaneous fibrolipoma is a rare neoplasm originating from hypertrophy of mature fat and fibrous connective tissue.[1–3] There have been few reports describing radiological findings of subcutaneous fibrolipoma.[1,2] We report a case of subcutaneous fibrolipoma in the upper back, and we highlight the radiological findings.

Case report

A 65-year-old man was admitted to our hospital because of a subcutaneous mass in his upper back. Three years earlier, he had noticed a firm, small, painless subcutaneous mass on the upper back. The mass had become markedly enlarged over the previous 1-year period. The patient was in his usual state of good health before admission. On physical examination, a well-circumscribed, freely movable giant subcutaneous mass, approximately 15cm in diameter, was palpated in the upper back.

Computed tomography (CT) showed a huge heterogeneous hypodensity mass located in the subcutaneous fat tissue (Fig. 1). The mass consisted predominantly of fat density interspersed with and surrounded by scattered soft tissue density areas, which were gradually enhanced on the delayed phase of contrast-enhanced CT. There was no distinct calcification or necrosis in the tumor. On magnetic resonance imaging (MRI), the mass showed mixed heterogeneous high intensity identical to that of the subcutaneous adipose tissue and low intensity on both T1-weighted (TR/TE, 300–450/9–14ms) and T2-weighted (TR/TE, 4000/97–105ms) images (Fig. 2). On gadolinium-enhanced T1-weighted images, the tumor shows heterogeneous enhancement. The ^{99m}Tc-HMDP (hydroxymethylenediphosphonate) bone scan and thallium-201(^{201}Tl) scintigram showed faint extraskeletal uptake in the tumor (Fig. 3).

M. Kajihara · Y. Sugawara (✉) · H. Miki · T. Mochizuki
Department of Radiology, Ehime University School of Medicine, Shitsukawa, Toon, Ehime 791-0295, Japan
Tel. +81-89-960-5371; Fax +81-89-960-5375
e-mail: sugawara@m.ehime-u.ac.jp

K. Sakayama
Department of Orthopaedic Surgery, Ehime University School of Medicine, Ehime, Japan

Y. Abe
Department of Pathology, Ehime University School of Medicine, Ehime, Japan

This case was presented in part at the 101st meeting of the Chugoku-Shikoku Regional Chapter of the Japanese Radiological Society, Yonago, December 2004.

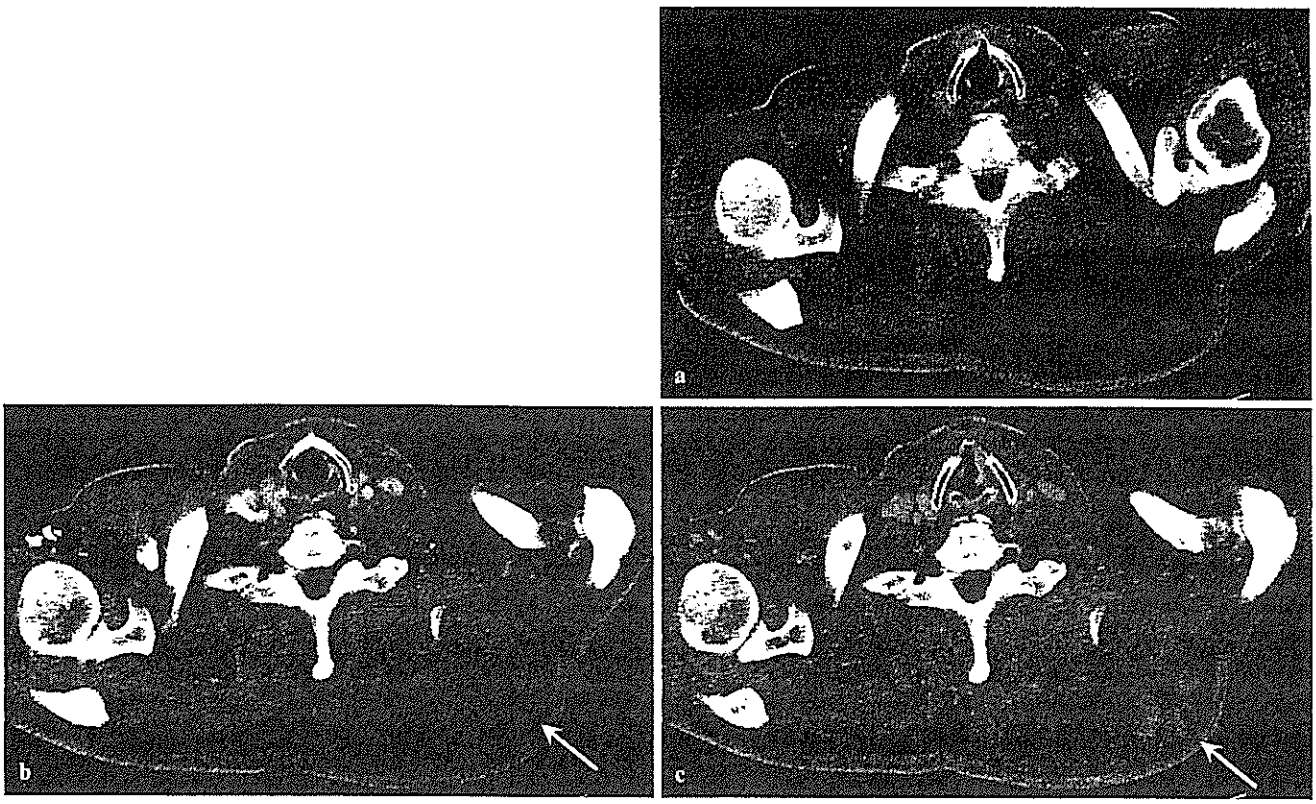

Fig. 1. **a** Precontrast axial computed tomography (CT) image shows a hypodense fatty tumor interspersed within isodense areas in the back. **b** On the arterial phase of a post-contrast-enhanced CT image (30 s after injection), nonadipose areas are enhanced slightly (*arrow*). **c** On the delayed phase of a post-contrast-enhanced CT image (120 s after injection), an irregular globular area of nonadipose part is enhanced (*arrow*)

Based on these findings, a malignant or intermediate lipomatous neoplasm such as a well-differentiated liposarcoma or a benign lipomatous tumor such as spindle cell lipoma or pleomorphic lipoma was suspected. At surgery, the tumor was resected with underlying trapezius muscle in en bloc. The tumor was easily separated from the scapula and did not involve the brachial plexus. Macroscopically, the tumor was firm, yellowish, and did not demonstrate necrotic or hemorrhagic areas (Fig. 4a). Histopathological sections showed mature adipocytes intermixed with abundant collagen fibers. There were no immature adipocytes, lipoblasts, spindle cells, or multinucleated giant cells. Therefore, the tumor was finally diagnosed as fibrolipoma (Fig. 4b).

Discussion

The lipoma is occasionally altered by the admixture of other mesenchymal elements that are an intrinsic part of it. The most abundant of these elements is fibrous connective tissue.[2] When significant fibrous tissue is present, these lesions may be termed fibrolipomas based on their pathology.[3] There have been some reports of these growths in the oral cavity, parotid gland and esophagus, intestine, and other areas.[4–9] However, few reports have described the radiological findings of this tumor, especially in subcutaneous sites.[2]

On MR images, the signal intensity of fatty and nonfatty tissues was characteristic on T1-weighted and T2-weighted images. Kim et al. reported that a central, nonfatty, ovoid region in the fibrolipoma did not show any enhancement.[2] In the current case, however, inhomogeneous moderate enhancement in nonfatty (fibrous) regions was observed. Before surgery, spindle cell or pleomorphic lipomas and well-differentiated liposarcomas were initially considered in the differential diagnosis. Especially, spindle cell lipoma was considered, as it preferably occurs in men 45–60 years of age in the subcutaneous tissue of the posterior neck, shoulder, and back.[3] Moreover, in spindle cell lipomas, nonfatty regions appear as areas of soft tissue density on nonenhanced CT and are well enhanced on contrast-enhanced CT.[2] However, in the histopathological examination of resected specimens, there were no immature

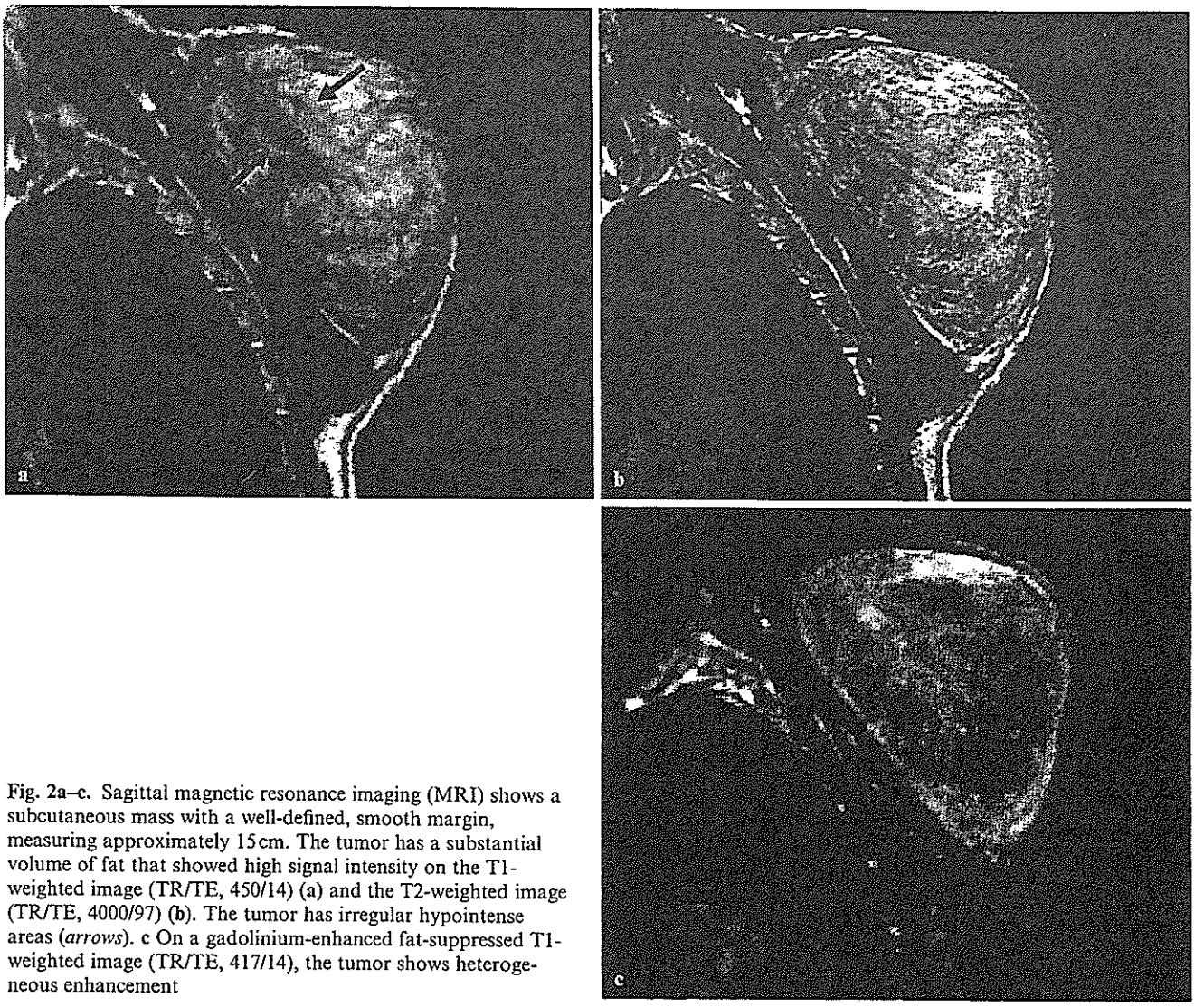

Fig. 2a–c. Sagittal magnetic resonance imaging (MRI) shows a subcutaneous mass with a well-defined, smooth margin, measuring approximately 15 cm. The tumor has a substantial volume of fat that showed high signal intensity on the T1-weighted image (TR/TE, 450/14) (**a**) and the T2-weighted image (TR/TE, 4000/97) (**b**). The tumor has irregular hypointense areas (*arrows*). **c** On a gadolinium-enhanced fat-suppressed T1-weighted image (TR/TE, 417/14), the tumor shows heterogeneous enhancement

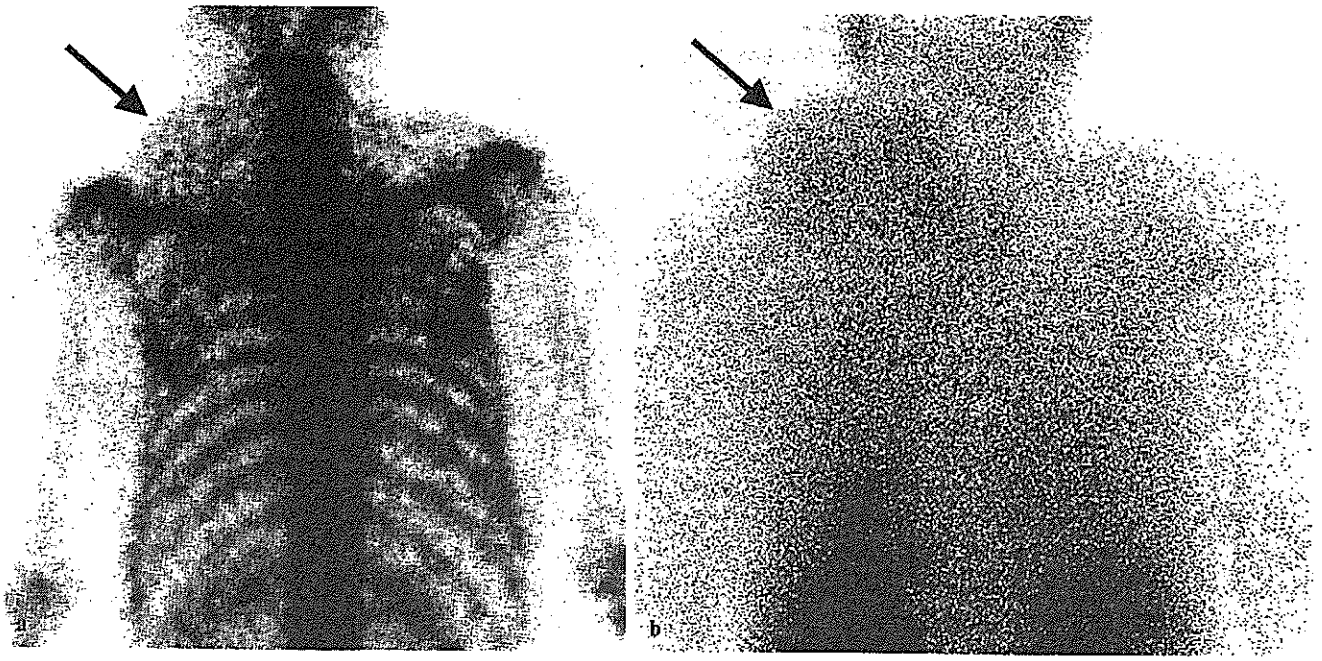

Fig. 3. **a** Posterior view of ^{99m}Tc-HMDP bone scintigraphy demonstrates faint extraskeletal uptake in the mass (*arrow*). **b** Posterior view of ^{201}Tl scintigraphy shows homogeneous faint uptake in the mass (*arrow*)

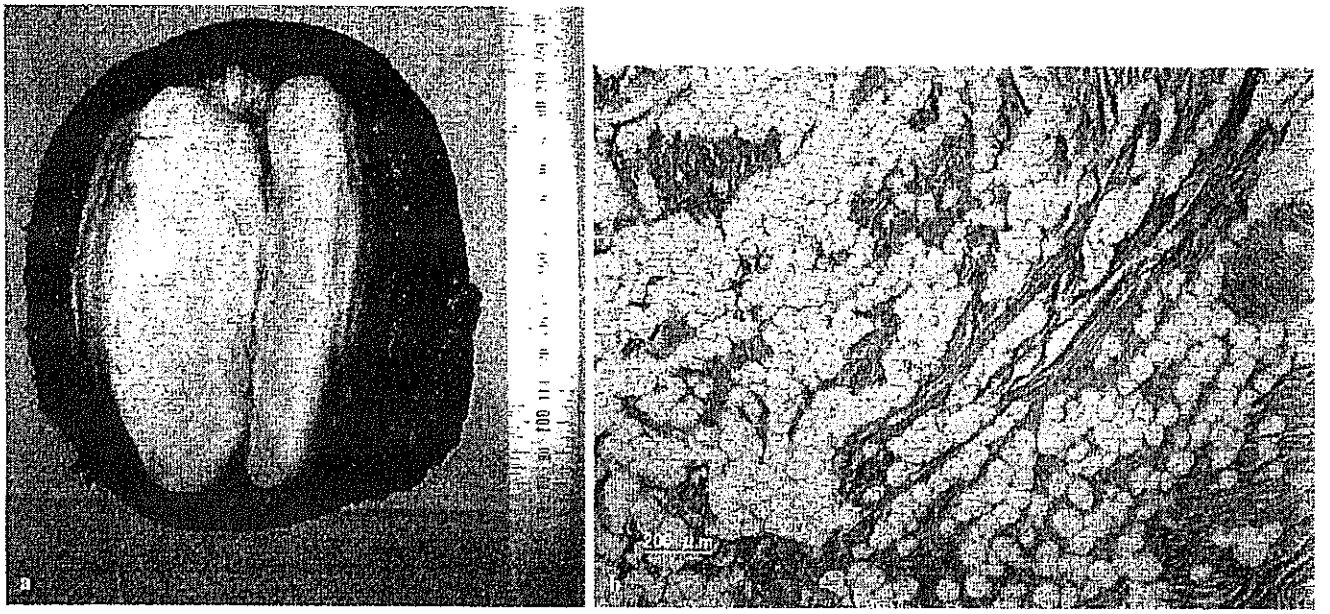

Fig. 4a,b. Cross section of the tumor: gross appearance and histopathological features. **a** Grossly, the tumor is well demarcated and yellow; it consists of fatty components. **b** Histopathological sections show massive mature adipocytes intermixed with abundant collagen fibers, but there are no immature adipocytes, lipoblasts, spindle cells, or multinucleated giant cells. These findings are consistent with a fibrolipoma. (H&E, ×100)

adipocytes, lipoblasts, spindle cells, or multinucleated giant cells, so the tumor was finally diagnosed as a fibrolipoma.

Hosono et al. reported that if the tumor has well-enhanced septa with a maximum width of >2 mm as well as irregular width and bulging confluence, the tumor is suggested to be malignant. However, there are several benign lipomatous tumors that might become well and diffusely enhanced.[10] Ohguri et al. indicated that most lipomatous tumors with thin septa were benign lipomas; but 2 were well-differentiated liposarcomas and 7 of 32 (22%) of the benign lipomas showed thick septa (>2 mm), and a nodular or patchy nonadipose component was detectable in 3 of the 32 (9%).[11] In a recent review of 60 lipomatous tumors (35 lipomas and 25 well-differentiated liposarcomas), the average largest dimension of well-differentiated liposarcomas was nearly twice that of benign lipomas (24 vs 13 cm), and patients with liposarcoma were older than those with lipoma (65 vs 52 years).[12] Thick septa or nodular areas are significant predictors of malignancy along with nonadipose tissue comprising more than 25% of the lesion.[12] Our case was unique because the tumor showed linear and reticulated fibrous tissue interspersed with a fatty component, and the fibrous nonadipose component became considerably enhanced after administration of contrast medium, promoting the confusion with a liposarcoma.

In musculoskeletal tumors, ^{201}Tl scintigraphy has been reported to be useful for differentiating benign from malignant tumors. Terui et al. reported that almost all lipomas showed no ^{201}Tl uptake, whereas 80% of liposarcomas showed uptake of ^{201}Tl.[13] In the current case, the tumor showed faint ^{201}Tl uptake, which also made the differential diagnosis from liposarcoma difficult.

In the current case report, CT images demonstrated nonadipose areas within the tumor that were moderately enhanced on the delayed phase compared with the early phase after administration of contrast medium. Generally, it is thought that an area showing slow enhancement has poor cellularity. In the dynamic contrast-enhanced MRI studies, Verstraete et al. reported that a significant difference was found between first-pass slope values of benign and malignant lesions.[14] Recently, Tuncbilek et al. reported that the steepest slope of the enhancement curve for liposarcomas was larger than that for lipomas.[15] Thus, the enhancement pattern after administration of contrast medium may provide useful information for differentiating fibrolipoma from liposarcoma, although more clinical experiences are needed.

References

1. Kransdorf MJ, Murphey MD. Lipomatous tumors: imaging of soft tissue tumors. Philadelphia: Saunders; 1997. p. 57–101.
2. Kim JY, Park JM, Lim GY, Chun KA, Park YH, Yoo JY. Atypical benign lipomatous tumors in the soft tissue: radio-

graphic and pathologic correlation. J Comput Assist Tomogr 2002;26:1063–8.
3. Weiss SW, Goldblum JR. Benign lipomatous tumors. In: Strauss M (ed): Enzinger and Weiss's soft tissue tumors. 4th edition. St. Louis: Mosby; 2001. p. 571–639.
4. De Visscher JG. Lipomas and fibrolipomas of the oral cavity. J Maxillofac Surg 1982;10:177–81.
5. Saitoh Y, Hama T, Ishizaka S, Kawaguchi M, Terazono T, Hyuga M, et al. Fibrolipoma of the parotid in a child. Am J Otolaryngol 1995;16:433–5.
6. Migliore M, Jeyasingham K. Pedunculated intraluminal oesophageal fibrolipoma: a case report. J Cardiovasc Surg (Torino) 1998;39:519–21.
7. Kawamoto K, Masuda K, Tsuneyoshi M. Fibrolipoma (lipoma) of the intestine. Nippon Rinsho Suppl 1994;6:502–4.
8. Hegele A, Olbert P, Roessler M, Heidenreich A, Hofmann R. Inguinal fibrolipoma of the spermatic cord: discrepancies between clinical and histopathological findings. Urol Int 2003;71:435–6.
9. Hsu JS, Kang WY, Liu GC, Kao EL, Chuang MT, Chou SH. Giant fibrolipoma in the mediastinum: an unusual case. Ann Thorac Surg 2005;80:e10–2.
10. Hosono M, Kobayashi H, Fujimoto R, Kotoura Y, Tsuboyama T, Matsusue Y, et al. Septum-like structures in lipoma and liposarcoma: MR imaging and pathologic correlation. Skeletal Radiol 1997;26:150–4.
11. Ohguri T, Aoki T, Hisaoka M, Watanabe H, Nakamura K, Hashimoto H, et al. Differential diagnosis of benign peripheral lipoma from well-differentiated liposarcoma on MR imaging: is comparison of margins and internal characteristics useful? AJR Am J Roentgenol 2003;180:1689–94.
12. Kransdorf MJ, Bancroft LW, Peterson JJ, Murphey MD, Foster WC, Temple HT. Imaging of fatty tumors: distinction of lipoma and well-differentiated liposarcoma. Radiology 2002;224:99–104.
13. Terui S, Terauchi T, Abe H, Fukuma H, Beppu Y, Chuman K, et al. On clinical usefulness of Tl-201 scintigraphy for the management of malignant soft tissue tumors. Ann Nucl Med 1994;8:55–64.
14. Verstraete KL, De Deene Y, Roels H, Dierick A, Uyttendaele D, Kunnen M. Benign and malignant musculoskeletal lesions: dynamic contrast-enhanced MR imaging—parametric "first-pass" images depict tissue vascularization and perfusion. Radiology 1994;192:835–43.
15. Tuncbilek N, Karakas HM, Okten OO. Dynamic contrast enhanced MRI in the differential diagnosis of soft tissue tumors. Eur J Radiol 2005;53:500–5.

Thallium-201 SPECT in prognostic assessment of malignant gliomas treated with postoperative radiotherapy

Takatoshi SEMBA, Yoshifumi SUGAWARA, Takashi OCHI, Takashi FUJII,
Teruhito MOCHIZUKI and Takanori OHNISHI

Reprint from Annals of Nuclear Medicine Vol. 20 No. 4
May 2006

ORIGINAL ARTICLE

Annals of Nuclear Medicine Vol. 20, No. 4, 287–294, 2006

Thallium-201 SPECT in prognostic assessment of malignant gliomas treated with postoperative radiotherapy

Takatoshi SEMBA,* Yoshifumi SUGAWARA,* Takashi OCHI,* Takashi FUJII,* Teruhito MOCHIZUKI* and Takanori OHNISHI**

*Department of Radiology, Ehime University School of Medicine
**Department of Neurosurgery, Ehime University School of Medicine

Objective: This study was designed to investigate the value of preoperative thallium-201 (^{201}Tl) SPECT as a predictor of outcome in malignant glioma. ***Methods:*** From January 1990 to September 2003, 109 patients with glioma were treated with postoperative radiotherapy. Of these, 36 patients with malignant gliomas who underwent preoperative ^{201}Tl-SPECT were included in this study (grade 3: n = 14, grade 4: n = 22). On early (10 minutes) and delayed (2 hours) images after 111 MBq ^{201}TlCl injection, we calculated radioactivity ratios of tumors to contralateral normal brain (T/N ratios) and retention indices (RIs). For early and delayed images, we compared outcome between a high T/N ratio group (T/N ratio equal or greater than the average) and a low T/N ratio group (T/N ratio less than the average). We also divided the patients into two groups on the basis of RI; a high RI group (RI equal or greater than the average) and a low RI group (RI less than the average), and similarly compared outcome between the two groups. ***Results:*** Median survival time was 12 months for both grade 3 and grade 4 tumors; however, two-year survival was 53% for grade 3 and 15% for grade 4. In both early and delayed images, outcome was significantly better for patients with low T/N ratios (early <4.71, delayed <3.96) than those with high T/N ratios (early: $p = 0.030$, delayed: $p = 0.049$). However, no significant survival difference was apparent between the low- (< −12.25) and high RI groups. In grade 3 glioma, patients with high T/N ratios demonstrated a tendency toward poorer outcome, although this trend was not significant (early: $p = 0.079$, delayed: $p = 0.099$). Overall outcome was poor for grade 4 glioma, and the difference in survival between low and high T/N ratio groups was not significant (early: $p = 0.51$, delayed: $p = 0.53$). However, long survival was seen only in patients with lower T/N ratios. ***Conclusions:*** Differences of ^{201}Tl uptake in malignant gliomas could predict outcome. ^{201}Tl-SPECT is potentially useful in the management of patients with malignant gliomas.

Key words: glioma, thallium-201, SPECT, radiotherapy, prognosis

INTRODUCTION

DESPITE RECENT PROGRESS in imaging and treatment, the overall survival of patients with malignant glioma has not improved.[1] Several prognostic factors are well known to influence survival in this condition; such as performance status, age, tumor grade and histology, tumor size, and extent of surgery.[2–4] Histological grade has been considered an important prognostic factor; however, there can be discrepancies between grade and prognosis. A reliable preoperative predictor of prognosis would therefore be useful in determining intensive treatment including radiotherapy and chemotherapy.

CT and MR imaging with contrast are excellent imaging techniques used at most centers to evaluate gliomas. These methods mainly assess morphologic abnormalities. Recently, some authors have reported prognostic assessment using perfusion MR or MR spectroscopy (MRS).[5,6] However, there may be difficulties in defining

Received December 22, 2005, revision accepted February 20, 2006.

For reprint contact: Takatoshi Semba, M.D., Department of Radiology, Ehime University School of Medicine, 454, Shitsukawa, Toon, Ehime 791–0295, JAPAN.

tumor extension and grade, or differentiating tumor recurrence from necrosis or scar in particular areas.[7,8]

Thallium-201 chloride (^{201}Tl) scintigraphy has been widely used to detect various tumors and to differentiate benign from malignant lesions in the lung and thyroid.[9,10] ^{201}Tl scintigraphy has been reported useful for differentiating low grade from high grade gliomas and for distinguishing residual or recurrent viable gliomas from post-therapeutic changes such as radiation necrosis.[4,11–19] However, the association between preoperative ^{201}Tl accumulation in malignant glioma and prognosis after postoperative radiotherapy has not been adequately investigated.

In the present study, we investigated whether preoperative ^{201}Tl-SPECT could predict prognosis in patients with malignant glioma.

MATERIALS AND METHODS

Patients

From January 1990 to September 2003, 109 patients with glioma were treated with postoperative radiotherapy. Of these, 77 patients had been histologically diagnosed with malignant glioma (World Health Organization [WHO] grade 3 and grade 4). From this group, 36 patients (23 males, 13 females) who had all undergone ^{201}Tl-SPECT before surgery were included in this study. The other 41 patients did not undergo ^{201}Tl-SPECT before surgery because of their performance status, and/or their treatment schedules. Histological type was confirmed by examination of surgical specimens in all patients. All of them were malignant astrocytomas. Thirty-two tumors were located in supratentorial, 2 in cerebellum, and 2 in brain stem. Patient characteristics are shown in Table 1.

All patients had undergone postoperative conventionally fractionated external-beam radiotherapy (EBRT) with or without chemotherapy. Thirty-three patients had received limited field EBRT (with margins around enhancing lesions in the order of 2 cm), and 3 patients had undergone EBRT with whole brain fields. Median radiation dose was 50 Gy (range, 27.5–60 Gy) in daily fractions of 2–2.5 Gy. Thirty-two patients had undergone combined EBRT and chemotherapy after surgery. Chemotherapy regimens were changed in 2000. From 1990 to 1999, 20 patients were treated with nimustine hydrochloride transcatheter arterial infusion. After 2000, 12 patients were treated with carboplatin and etoposide intravenous infusion.

Table 1 Summary of patient characteristics

Histological grade		(n)
	grade 3	14
	grade 4	22
Gender		(n)
	male	23
	female	13
Age		(n)
	< 65 years	25
	≥ 65 years	11
	median	56 years
	range	12–76 years
KPS		(n)
	< 70	14
	≥ 70	22
Radiotherapy dose		(n)
	< 50 Gy	5
	50 Gy	22
	60 Gy	9
Follow-up*		(months)
	median	12
	range	0.8–103

KPS; Karnofsky performance status
* Duration from end of radiotherapy

Imaging

SPECT imaging was started at 10 minutes (early) and 2 hours (delayed) after 111 MBq of ^{201}Tl injection. SPECT imaging was performed using a four-head gamma camera (SPECT2000H-40, Hitachi Medical Corp., Tokyo, Japan) equipped with a low-energy, general-purpose collimator (until February 1999) and a three-head gamma camera (GCA9300-A, Toshiba Medical Corp., Tokyo, Japan) equipped with a low-energy, high-resolution collimator (from March 1999). Data were acquired with a 64 × 64 matrix, 20 seconds per projection for 64 projections in the four-head gamma camera, and with a 128 × 128 matrix, 75 seconds per projections for 45 projections (15 projections in each of three cameras) in the three-head gamma camera. Transaxial images were reconstructed by filtered back-projection with Ramp and Butterworth filters (cut-off 0.25/cm, order 10 in the four-head gamma camera, and cut-off 0.10/cm, order 8 in the three-head gamma camera). Attenuation correction was not performed.

Data Analysis

The axial slice with the highest count activity within the lesion identified on MR imaging or CT was chosen for quantitative analysis. A circular region of interest (ROI) was placed manually over the lesion on the slice showing greatest activity. The size of ROI was variably defined as surrounding the greatest activity area in the tumor. The contralateral ROI was drawn as a mirror image of the lesion ROI and manually moved in the area of presumably healthy brain. When the tumor was located in the midline area, the contralateral ROI was manually placed in the normal brain surrounding the tumor. Radioactivity ratios of tumors to contralateral normal brain (T/N ratios) were thus calculated; if accumulation of tracer in the tumor was not detected, the T/N ratio was defined as 1.

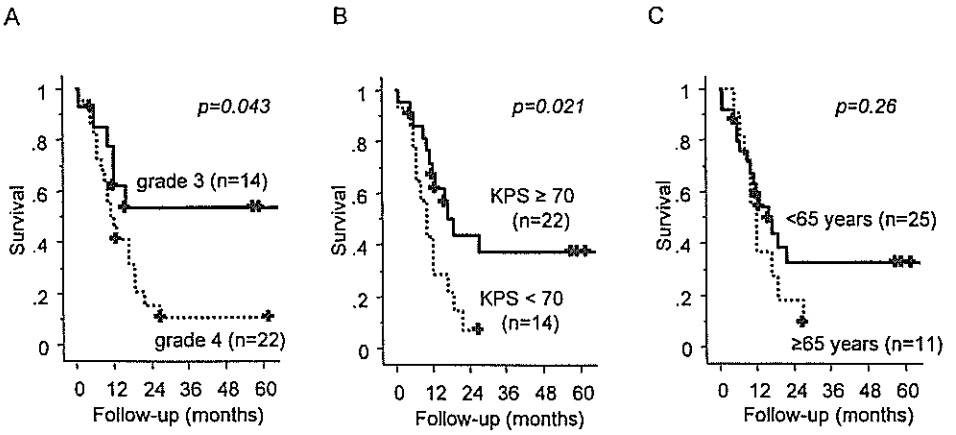

Fig. 1 Kaplan-Meier cumulative survival curves from the end of radiotherapy in all patients with malignant glioma according to histological grade (grade 3 vs. grade 4) (A), Karnofsky performance status (KPS, <70 vs. ≥70) (B), and age.(<65 years vs. ≥65 years) (C). Differences between the survival curves were assessed by the log-rank test.

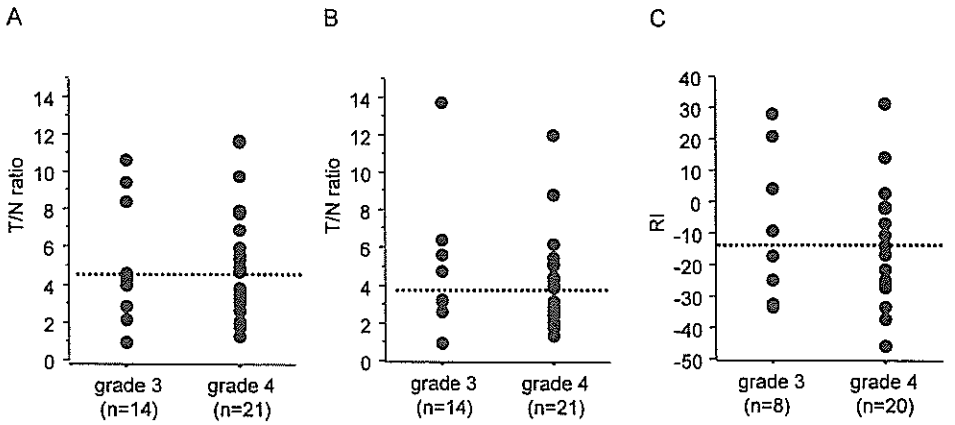

Fig. 2 Scattergrams of early T/N ratios (A), delayed T/N ratios (B), and retention indices (RIs) (C). Dashed lines represent mean values.

Patients were divided into two groups for early and for delayed images; those with low T/N ratios (less than the average T/N ratio) and those with high T/N ratios (equal or greater than the average T/N ratio). We compared outcome between these groups. Retention index (RI) was calculated as follows: RI = (delayed T/N – early T/N)/ early T/N × 100 (%). We also divided the patients into two groups with respect to RI, a low RI group (RI less than the average) and a high RI group (RI equal or greater than the average), and compared outcome between them. Of the patients with grade 4 glioma, early SPECT data were not available in one case due to patient movement, and delayed SPECT data were not available in another case because of the treatment schedule. As RI could not be calculated when no definite tumor accumulation of ^{201}Tl was appreciated and when early or delayed ^{201}Tl-SPECT data were unavailable, RI was calculated for 28 patients. We also investigated the relationship of outcome to the following clinical variables: histological grade (grade 3 or grade 4), gender (male or female), age (<65 years or ≥65 years), Karnofsky performance status (KPS) (<70 or ≥70), total irradiation dose (<50 Gy, 50 Gy, or 60 Gy), and concurrent chemotherapy (with or without).

Survival duration was measured from the end of radiotherapy. Cumulative survival rates were obtained using the Kaplan-Meier method and compared using the log-rank test, p values less than 0.05 were considered statistically significant. The interaction of each prognostic factor and its effect on survival was using the Cox proportional hazards model. Crude and adjusted rate ratios and their 95% CIs were calculated. Statistical analysis was performed with StatView for Windows version 5.0 (SAS Institute Inc., Cary, NC).

RESULTS

Significant differences were evident in outcome between the histological grades (Fig. 1). Median survival time was

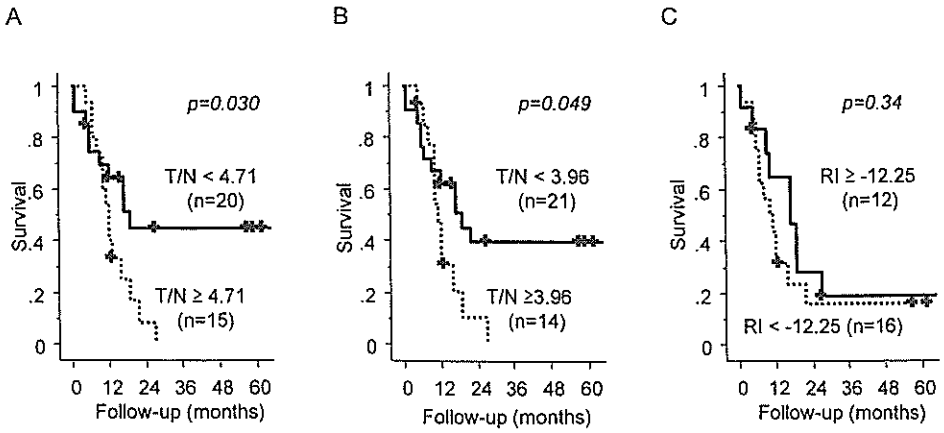

Fig. 3 Kaplan-Meier cumulative survival curves from the end of radiotherapy in all patients with malignant glioma, according to presence of low vs. high T/N ratios (early (A), delayed (B)), and RIs (C). Differences between the survival curves were assessed by the log-rank test.

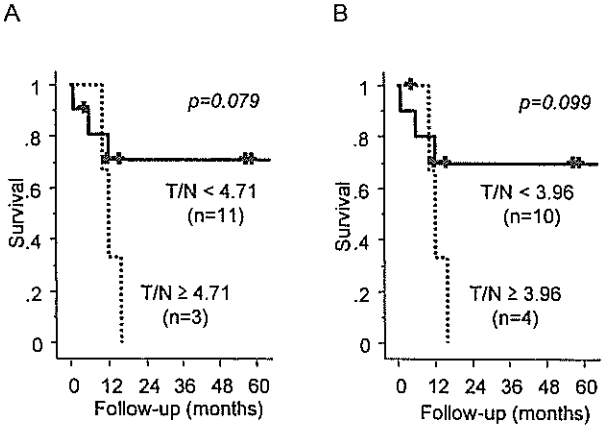

Fig. 4 Kaplan-Meier cumulative survival curves from the end of radiotherapy in patients with grade 3 glioma, according to presence of low vs. high T/N ratios (early (A), delayed (B)). Differences between the survival curves were assessed by the log-rank test.

12 months in both grades; however, two-year survival was 53% in grade 3 and 15% in grade 4. Neither gender ($p = 0.71$), age ($p = 0.26$), total irradiation dose ($p = 0.16$), nor concurrent chemotherapy ($p = 0.084$) affected survival; however, higher KPS was associated with longer survival than lower KPS ($p = 0.021$) (Fig. 1).

Mean T/N ratio was 4.71 in the early images and 3.96 in the delayed images. Both early and delayed T/N ratios exhibited wide variance, and substantial overlap of T/N ratio was found between grade 3 and grade 4. Mean RI was −12.25. Wide variance in RI was also evident (Fig. 2).

In both early and delayed images, patients with low T/N ratios had a significantly better outcome than those with high T/N ratios (early: $p = 0.030$, delayed: $p = 0.049$, Fig. 3). For example, using early T/N ratios, two-year survival rate was 45% in the low T/N group but only 8.3% in the high T/N group. No significant difference in survival was

Table 2 Summary of 3 patients with grade 3 glioma showing high T/N ratios on both early and delayed ^{201}Tl-SPECT images

	Patient 1	Patient 2	Patient 3
Histological grade	3	3	3
Gender	male	male	male
Age (years)	68	71	12
KPS	60	60	90
Early T/N ratio	10.72	9.54	8.49
Delayed T/N ratio	13.79	6.51	5.72
Retention index (%)	28.64	−31.76	−32.63
Radiation dose (Gy)	50	50	50
Prognosis (months)*	10	12	16

KPS; Karnofsly performance status
* Duration from end of radiotherapy

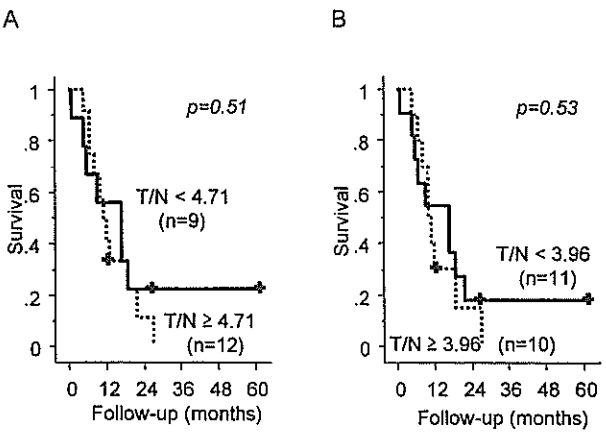

Fig. 5 Kaplan-Meier cumulative survival curves from the end of radiotherapy in patients with grade 4 glioma, according to presence of low vs. high T/N ratios (early (A), delayed (B)). Differences between the survival curves were assessed by the log-rank test.

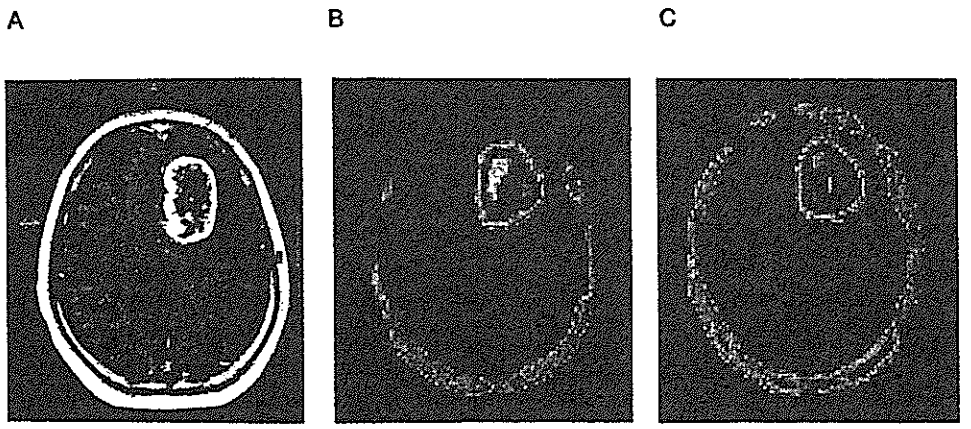

Fig. 6 A 56-year-old man with glioblastoma (grade 4) in the left frontal lobe. MR image before therapy shows a ring-like well-enhanced lesion on gadolinium contrast-enhanced T1-weighted image (Gd-T1WI) (A). Intense tumor uptake with high T/N ratios (early: 9.88, delayed: 6.25) was seen on both the early (B) and the delayed (C) ^{201}Tl-SPECT images. Total tumor resection and postoperative external beam irradiation (total 50 Gy) were performed, but this patient died of related disease 10 months after radiotherapy.

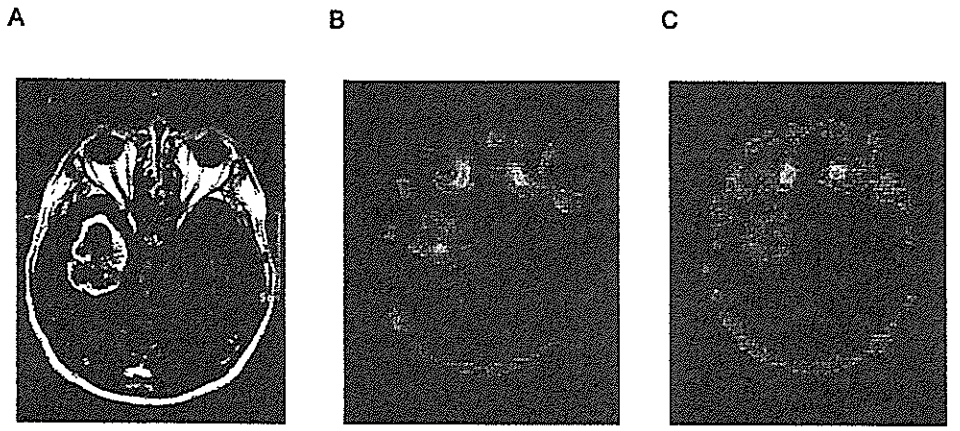

Fig. 7 A 64-year-old man with glioblastoma (grade 4) in the right temporal lobe (Table 3; Patient 2). MR image before therapy shows a ring-like well-enhanced lesion on gadolinium contrast-enhanced T1-weighted image (Gd-T1WI) (A). Tumor uptake was seen on both the early (B) and the delayed (C) ^{201}Tl-SPECT images, but the T/N ratios of 3.87 and 2.93 fell within the low T/N ratio group. Subtotal tumor resection and postoperative external beam irradiation (total 50 Gy) were performed, and this patient remains alive at 62 months after radiotherapy.

evident between the low-RI group and high-RI group ($p = 0.34$).

Although the difference was not significant (early: $p = 0.079$, delayed: $p = 0.099$) in patients with grade 3 glioma, patients with high T/N ratios had a tendency toward poorer prognosis (Fig. 4). Two-year survival rates in patients with low T/N ratios were 71% for the early images and 70% for the delayed images, while all patients with high T/N ratios died within 16 months (Table 2).

In patients with grade 4 glioma, overall prognosis was poor, and no significant difference was evident between the high- and low-T/N groups (early: $p = 0.51$, delayed: $p = 0.53$) (Fig. 5). However, in both early and delayed images, long survival was only seen in patients with lower T/N ratios (Table 3). There are representative cases in Figure 6 and Figure 7. These two patients with grade 4 glioma showed a similar enhanced pattern on gadolinium contrast-enhanced T1-weighted MR images; however, one (Fig. 6) died 10 months after radiotherapy and his preoperative ^{201}Tl-SPECT showed high T/N ratios, while the other (Table 3; Patient 2, Fig. 7) remains alive at 62 months after radiotherapy and his preoperative ^{201}Tl-SPECT showed low T/N ratios.

In univariate analysis, significant differences were seen

Table 3 Summary of 2 patients with grade 4 glioma showing low T/N ratios on both early and delayed ^{201}Tl-SPECT images

	Patient 1	Patient 2
Histological grade	4	4
Gender	female	male
Age (years)	76	64
KPS	60	70
Early T/N ratio	2.13	3.87
Delayed T/N ratio	2.11	2.93
Retention index (%)	−0.94	−24.29
Radiation dose (Gy)	50	50
Outcome (months)*	27†	62†

KPS; Karnofsky performance status
* Duration from end of radiotherapy
† Alive

Table 4 Multivariate analysis of prognostic factors

		Rate ratio	95% CI	p Value
KPS	< 70	1.7	0.7–4.0	0.24
	≥ 70	1.0		
Histological grade	grade 3	0.6	0.2–1.7	0.33
	grade 4	1.0		
Early T/N ratio	High	1.7	0.7–4.2	0.25
	Low	1.0		

KPS; Karnofsky performance status

in KPS, histological grade, and T/N ratios, whereas multivariate analysis showed no significant difference (Table 4).

DISCUSSION

Several large trials have analyzed a wide range of prognostic factors in patients with malignant glioma, and these trials have consistently shown that age, performance status, mental status, tumor grade and histology, and extent of surgical resection are the most significant prognostic factors influencing survival.[3] Jeremic et al. reported that age, KPS, size, and extent of surgery were independent prognosticators of survival/progression-free survival.[2] The present study showed that while KPS was a statistically significant prognostic factor of survival, age was not (Fig. 1).

One of the important prognostic factors identified is tumor histological grade. However, discrepancies are often experienced in this regard. While the present study demonstrated histological grade to be a statistically significant prognostic factor, some patients with grade 3 glioma exhibited a poor outcome, while some patients with grade 4 tumors survived for a relatively long period.

^{201}Tl scintigraphy has been widely used to detect various tumors. ^{201}Tl SPECT has been reported to be a non-invasive tool not only for the detection of glioma but also for the prediction of both tumor type and histological grade.[11] However, while many previous ^{201}Tl SPECT studies have been directed at evaluating the therapeutic effect or detecting tumor recurrence,[11–16] the literature contains few reports regarding the usefulness of preoperative ^{201}Tl SPECT in evaluating post therapeutic prognosis.[17–20]

Previously, Oriuchi et al. reported a positive correlation between ^{201}Tl uptake and proliferation activity estimated by bromodeoxyuridine (BUdR) labeling and suggested that ^{201}Tl could potentially be an effective medium for characterizing tumor proliferation.[17] They also reported that mean ^{201}Tl index and BUdR-labeling index were significantly associated with patient death. However, they did not investigate the correlation between ^{201}Tl uptake and survival. Higa et al. reported that ^{201}Tl-SPECT results were correlated with histological grade and were correlated most closely with outcome, identifying a group at high risk of dying from the disease.[18] Their study investigated the correlation between ^{201}Tl uptake and survival; however they assessed the degree of ^{201}Tl uptake by visual grading. In addition, because Higa et al.'s study included low grade gliomas, it would appear inadequate for assessing differences in prognosis for malignant glioma. Kosuda et al. reported that the lesion/normal (L/N) ratio was very useful in predicting survival of patients with grade 3 glioma or a solitary cerebral metastasis, when evidence of a mass lesion persisted after the initial combined modality treatment. On the other hand, the L/N ratio did not predict survival of grade 4 glioma patients in whom a mass lesion was apparent after the initial combined modality treatment.[19] In our preoperative ^{201}Tl-SPECT study, patients with low T/N ratios demonstrated a significantly better outcome than those with high T/N ratios. In grade 3 glioma, patients with high T/N ratios exhibited a poorer outcome than those with low T/N ratios. In grade 4 glioma, although overall outcome was poor, long survival was only seen in patients with low T/N ratios.

^{201}Tl uptake may be related to a combination of factors including regional cerebral blood flow, blood brain barrier permeability, and cellular uptake that may involve transmembrane transport into viable tumor cells.[16,22] Some authors have commented that ^{201}Tl-SPECT delayed images and RI are useful in differentiating benign thyroid tumors and thoracic lesions from malignancy.[9,10] With regard to brain tumors, studies have demonstrated these indices to be useful,[21,22] but only in distinguishing low-grade from high-grade tumors. ^{201}Tl-SPECT delayed images and RI have not been shown to be valuable in distinguishing grade 3 from grade 4 glioma or in prediction of survival of malignant glioma. The present study investigated delayed ^{201}Tl-SPECT images; however, we could not demonstrate any superiority of delayed over early imaging. Hence, RI was not a significant predictor of survival in malignant glioma. Indeed many studies of ^{201}Tl-SPECT in malignant glioma mentioned only early

images.[4,12,14,15,17–20]

In the present study, overall outcome of patients with grade 4 glioma was poor; however, long survival was seen only in patients with low T/N ratio. Hence, ^{201}Tl-SPECT might reflect outcome better than histological grade. This might be explained by the fact that although resected specimens contained few aggressively malignant elements, pathologists classified tumors as grade 4. Accordingly, tumor accumulation of ^{201}Tl (in other words, T/N ratio in this study) appears to be averaged (reduced) when the proportion of tissue with higher uptake is small.

On the other hand, in grade 3 glioma, a clear trend was evident; patients with high T/N ratios exhibited a poorer outcome than those with low T/N ratios. The heterogeneous nature of glioma might lead to high histological sampling variation, thereby reducing the reliability of histological diagnosis.[20] For example, a patient with high T/N ratio (Table 2; Patient 1) was histologically diagnosed as having grade 3 glioma, but his post-therapeutic survival was poor. Postoperative MR imaging showed residual tumor at the site of a hot spot seen on preoperative ^{201}Tl-SPECT. It seems likely that the residual mass contained more malignant cells than the rest of the tumor, and hence grade might have been underestimated. We did not investigate the correlation between residual tumor and the site of hot spots on ^{201}Tl-SPECT in other individual cases. However, this might enable us to reduce discrepancies between histological grade and prognosis by recommending that the neurosurgeon performs biopsy as close as possible to the hot spot on ^{201}Tl-SPECT. Moreover, presence of residual tumor at the site of a hot spot on preoperative ^{201}Tl-SPECT, might justify increasing the focal dose of postoperative radiotherapy using stereotactic radiosurgery or intensity-modulated radiation therapy.[23,24]

Patients with high T/N ratios exhibited a poorer outcome than those with low T/N ratios in grade 3, but there was no significant difference in this study. Additionally, multivariate analysis could not show any independent prognostic factor. The smaller number of patients may be one of the limitations and have influenced the results. However, this study indicates that ^{201}Tl uptake in malignant glioma could predict outcome. Further investigation is needed.

Recently, perfusion MR, MR spectroscopy, and ^{11}C-methionine PET have been reported as prognostic markers in patients with gliomas.[5,6,25] Kim et al. reported that ^{11}C-methionine PET was an independent significant prognostic factor and ^{11}C-methionine uptake was correlated with cellular proliferation.[25] However, this study investigated about gliomas including low grade. About perfusion MR, Lev et al. reported that gadolinium-based relative cerebral blood volume (rCBV) maps could be a marker of high-grade glioma, and degree of normalized CBV elevation was a stronger predictor of both tumor grade and survival than was degree of enhancement.[5] In addition, Tarnawski et al. reported about MRS that the strongest prognostic factor was lactate/*N*-acetyl aspartate (NAA) ratio in postoperative patients with malignant gliomas.[6] Comparative studies of these modalities and ^{201}Tl-SPECT would be recommended.

CONCLUSION

In the present study, patients with low T/N ratios exhibited significantly better prognosis than those with high T/N ratios. In grade 3 glioma, patients with high T/N ratios exhibited a poorer outcome than those with low T/N ratios. In grade 4 glioma, long survival was only seen in patients with lower T/N ratios. These results indicate that ^{201}Tl uptake in malignant glioma could predict prognosis. Hence, ^{201}Tl-SPECT could potentially be useful in the management of malignant glioma.

ACKNOWLEDGMENTS

We would like to thank Kou Nakagawa, M.D., Department of Neurosurgery in our university. This study was presented in part at the 52nd annual meeting of the Society of Nuclear Medicine, Toronto, Ontario, Canada, June 18–22, 2005, and at the 91st scientific assembly and annual meeting of the Radiological Society of North America, Chicago, Illinois, USA, November 27–December 2, 2005.

REFERENCES

1. Brandes AA. State-of-the-art treatment of high-grade brain tumors. *Semin Oncol* 2003; 30 (6 suppl 19): 4–9.
2. Jeremic B, Milicic B, Grujicic D, Dagovic A, Aleksandrovic J. Multivariate analysis of clinical prognostic factors in patients with glioblastoma multiforme treated with a combined modality approach. *J Cancer Res Clin Oncol* 2003; 129: 477–484.
3. Buckner JC. Factors influencing survival in high-grade gliomas. *Semin Oncol* 2003; 30 (6 suppl 19): 10–14.
4. Vos MJ, Hoekstra OS, Barkhof F, Berkhof J, Heimans JJ, van Groeningen CJ, et al. Thallium-201 single-photon emission computed tomography as an early predictor of outcome in recurrent glioma. *J Clin Oncol* 2003; 21: 3559–3565.
5. Lev MH, Ozsunar Y, Henson JW, Rasheed AA, Barest GD, Harsh GR 4th, et al. Glial tumor grading and outcome prediction using dynamic spin-echo MR susceptibility mapping compared with conventional contrast-enhanced MR: confounding effect of elevated rCBV of oligodendrogliomas. *Am J Neuroradiol* 2004; 25: 214–221.
6. Tarnawski R, Sokol M, Pieniazek P, Maciejewski B, Walecki J, Miszczyk L, et al. ^{1}H-MRS *in vivo* predicts the early treatment outcome of postoperative radiotherapy for malignant gliomas. *Int J Radiat Oncol Biol Phys* 2002; 52: 1271–1276.
7. Ricci PE. Imaging of adult brain tumors. *Neuroimaging Clin N Am* 1999; 9: 651–669.
8. Vallejos V, Balaña C, Flaile M. Use of ^{201}Tl SPECT imaging to assess the response to therapy in patients with